Supplementary Information for:

Conformational Analysis of Peramivir Reveals Critical Differences Between Free and Enzyme-Bound States

MedChemComm 2014

Michele R. Richards,[b] Michael G. Brant,[a] Martin J. Boulanger,[c]
Christopher W. Cairo[b] and Jeremy E. Wulff*[a]

[a] Department of Chemistry, University of Victoria, Victoria British Columbia V8W 3V6, Canada. E-mail: wulff@uvic.ca.
[b] Alberta Glycomics Centre, Department of Chemistry, University of Alberta, Edmonton Alberta T6G 2G2, Canada.
[c] Department of Biochemistry and Microbiology, University of Victoria, Victoria British Columbia V8W 3V6, Canada.

Index

Experimental Methods

General procedures

Peramivir was purchased from D-L Chiral Chemicals. Sources of X-ray diffraction data were from the Cambridge Structure Database (CSD) under CCDC 641049;[S1] or the Protein Data Bank (PDB IDs: 2F10, 3K37, 3K39, 1L7F, 1L7G, 1L7H, 2HTU, 4MWV, and 4MX0.[S2,S3,S4,S5]

NMR Spectroscopy

The 1D solution-state ^{1}H NMR spectrum for peramivir was obtained in D_2O at 27 °C on a 700 MHz spectrometer equipped with a cryoprobe. A presaturation pulse sequence was used to reduce the intensity of the residual HOD signal (4.78 ppm at 27 °C). The ^{1}H–^{1}H coupling constants were determined using a combination of first-order analysis and simulation in SpinWorks[S6] as described previously.[S7]

2D NMR spectra, as well as nOe experiments, were performed at 500 MHz. For the nOe experiments, the D1 relaxation delay was set to 2 s, and the D8 mixing time was set to 0.65 s.

Computational methods

Molecular dynamics (MD) simulations on peramivir were run using the Generalized Amber Force Field[S8] and the PMEMD module of the AMBER 10 software suite.[S9] Peramivir was solvated in a box of 379 TIP3P[S10] water molecules with an initial size of 28.9 x 28.1 x 25.5 Å. Partial charges were calculated using the previously reported approach for restrained electrostatic potential (RESP) charge fitting,[S11,S12,S13] and all aliphatic hydrogens were assigned a charge of zero. The Generalized Amber Force Field did not contain the appropriate dihedral or improper torsion terms for the guanidine group, so these parameters were taken from the ff99SB force field.[S14]

Prior to the production phase, peramivir was equilibrated in a four-step process. First, the water molecules were minimized while holding peramivir fixed, then the entire system was minimized. For both rounds, 50 steps of steepest decent were followed by 950 step of conjugant gradient minimization. The system was then subjected to simulated annealing, heating from 5 K to 300 K over 50 ps and cooling back to 5 K over 50 ps. Final equilibration was run heating the system from 5 K to 300 K over 100 ps, then running at a constant 300 K for an additional 100 ps. Following equilibration, production dynamics were run for 250 ns at 300 K. The temperature was held constant using the Berendsen thermostat[S15] and rescaled every 1 ps. Pressure was held constant at 1 atm. All bonds containing hydrogen were fixed using the SHAKE algorithm.[S16] A 2 fs timestep was used for all dynamics steps, and the cutoff for nonbonding interactions was 8 Å. Nonbonded and electrostatic interactions were unscaled.

For the average coupling constants, 200 conformations were extracted from the MD simulation of peramivir. The Fermi contact term was then calculated for each conformation using B3LYP/6-31G(d,p) u+1s[S17,S18,S19] in Gaussian03,[S20] following the procedure of Bally and Rablen.[S21] The resulting $J_{H,H}$ values were averaged over all 200 conformations.

Figure S1: Comparison of Structural Properties for Free and Enzyme-Bound Oseltamivir

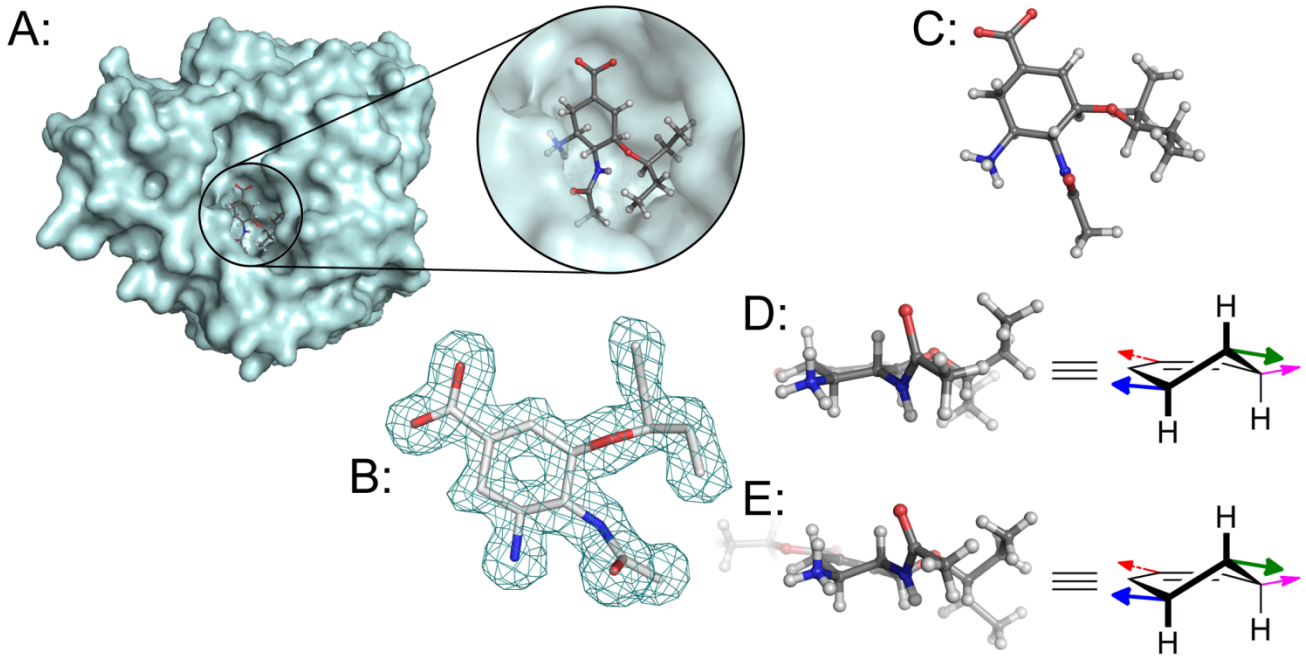

Figure S1. Comparison of structural properties for free and enzyme-bound oseltamivir, revealing a conserved geometry of the central ring. **A:** Oseltamivir carboxylate bound in the enzyme active site of H1N1 neuraminidase (from PDB 3TI6).[S22] **B:** Omit map for the bound ligand of PDB 3TI6, confirming the quality of the data for the bound ligand. **C** and **D:** Top- and side-views of the bound ligand from Figure S1A, showing the twist-boat conformation of the central ring. Colored arrows on the structural drawing correspond to the functional groups in Figure 1. Positions of hydrogen atoms are calculated based on the positions of the other atoms. **E:** Small-molecule X-ray data for oseltamivir (as the ethyl ester prodrug) from reference S23. Exocyclic bonds are rotated somewhat with respect to the enzyme-bound structure, but the geometry of the central core is largely preserved in the absence of binding.

Figure S2: Comparison of Structural Properties for Free and Enzyme-Bound Zanamivir

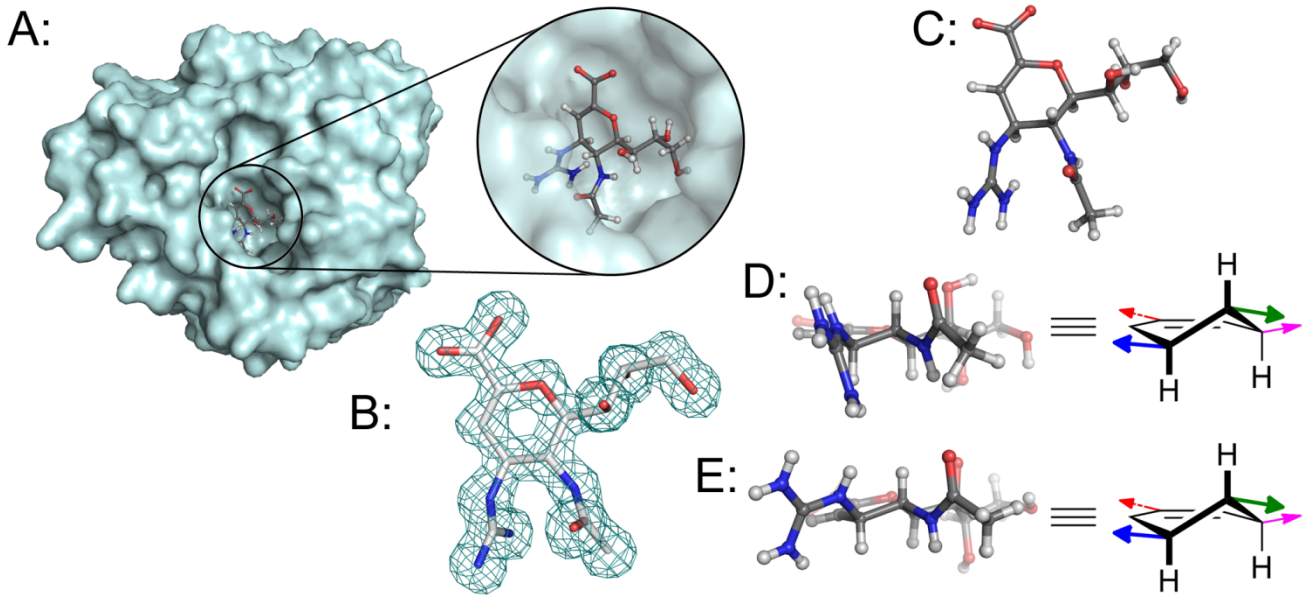

Figure S2. Comparison of structural properties for free and enzyme-bound zanamivir, revealing a conserved geometry of the central ring. **A:** Zanamivir bound in the enzyme active site of H1N1 neuraminidase (from PDB 3B7E).[S24] **B:** Omit map for the bound ligand of PDB 3B7E, confirming the quality of the data for the bound ligand. **C** and **D:** Top- and side-views of the bound ligand from Figure S2A, showing the twist-boat conformation of the central ring. Colored arrows on the structural drawing correspond to the functional groups in Figure 1. Positions of hydrogen atoms are calculated based on the positions of the other atoms. **E:** Small-molecule X-ray data for zanamivir (as a dimer) from reference S25. Exocyclic bonds are rotated somewhat with respect to the enzyme-bound structure, but the geometry of the central core is largely preserved in the absence of binding.

Figure S3: Comparison of Structural Properties for Free and Enzyme-Bound Peramivir

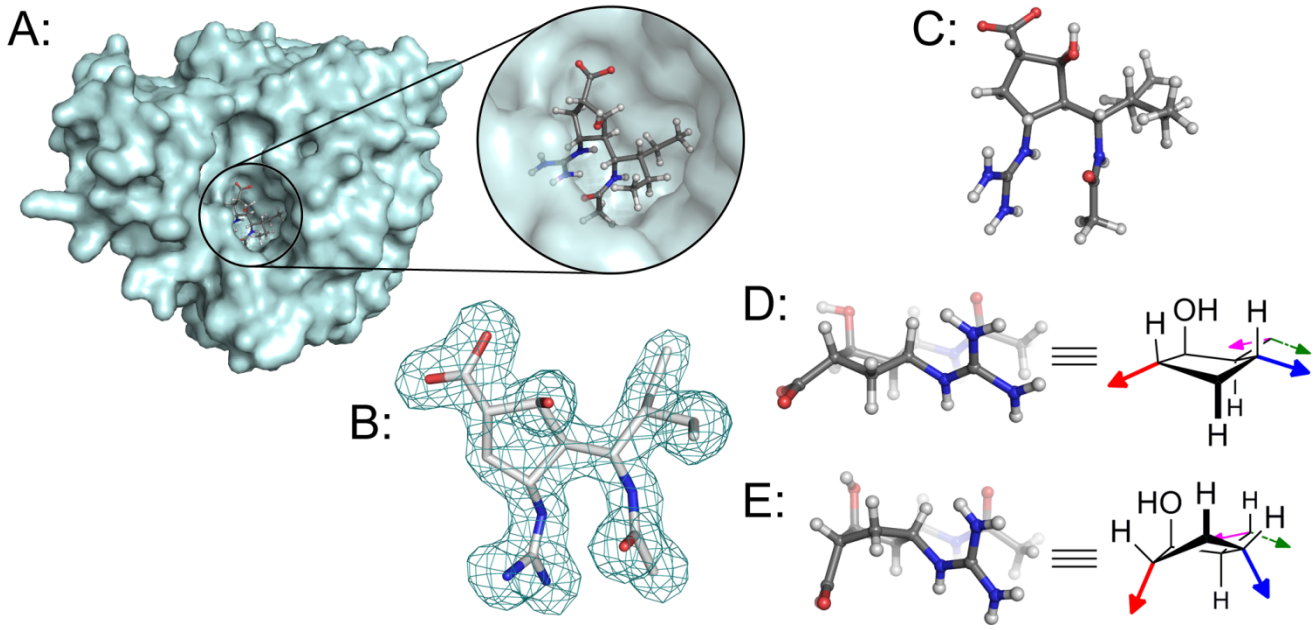

Figure S3. Comparison of structural properties for free and enzyme-bound peramivir, highlighting differences in the geometry of the central ring. **A:** Peramivir bound in the enzyme active site of H1N9 neuraminidase (from PDB 1L7F).[S3] **B:** Omit map for the bound ligand of PDB 1L7F, confirming the quality of the data for the bound ligand. **C** and **D:** Top- and side-views of the bound ligand from Figure S3A, showing the pronounced pseudo-equatorial projections of the carboxylate and guanidinium substituents. Colored arrows on the structural drawing correspond to the functional groups in Figure 1. Positions of hydrogen atoms are calculated based on the positions of the other atoms. **E:** Small-molecule X-ray data for peramivir from reference S1, showing a substantially different conformation.

Figure S4: Structural Properties for Peramivir Bound to Influenza B Neuraminidase

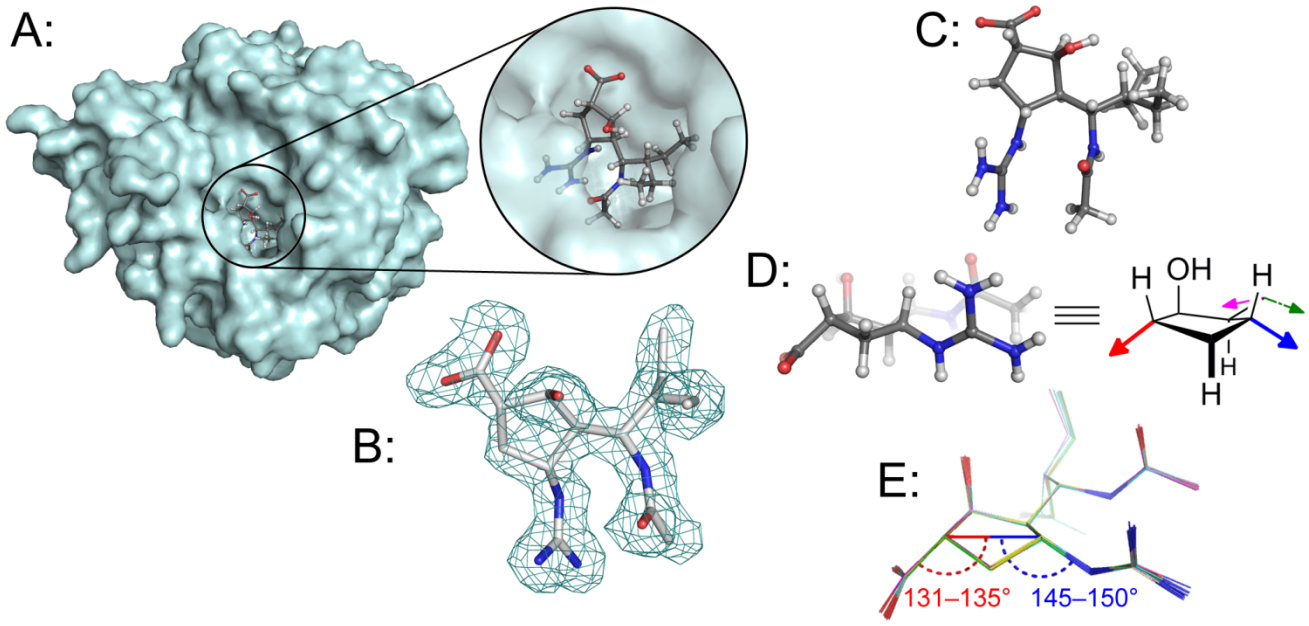

Figure S4. Structural properties for peramivir bound to influenza B neuraminidase. **A:** Peramivir bound in the enzyme active site of neuraminidase from influenza B/Perth/211/2001 (from PDB 3K37).[S5] **B:** Omit map for the bound ligand of PDB 3K37, confirming the quality of the data for the bound ligand. **C** and **D:** Top- and side-views of the bound ligand from Figure S4A, showing a relaxed geometry, relative to that shown in Figure S3C and D. Colored arrows on the structural drawing correspond to the functional groups in Figure 1. Positions of hydrogen atoms are calculated based on the positions of the other atoms. **E:** Overlay of all 18 different bound conformations of peramivir bound to either wild-type B/Perth neuraminidase (from PDB 3K37) or a D197E mutant (from PDB 3K39).[S5]

Figure S5: Comparison of Simulated and Experimental ^{1}H NMR Spectra for Peramivir (D_2O, 700 MHz)

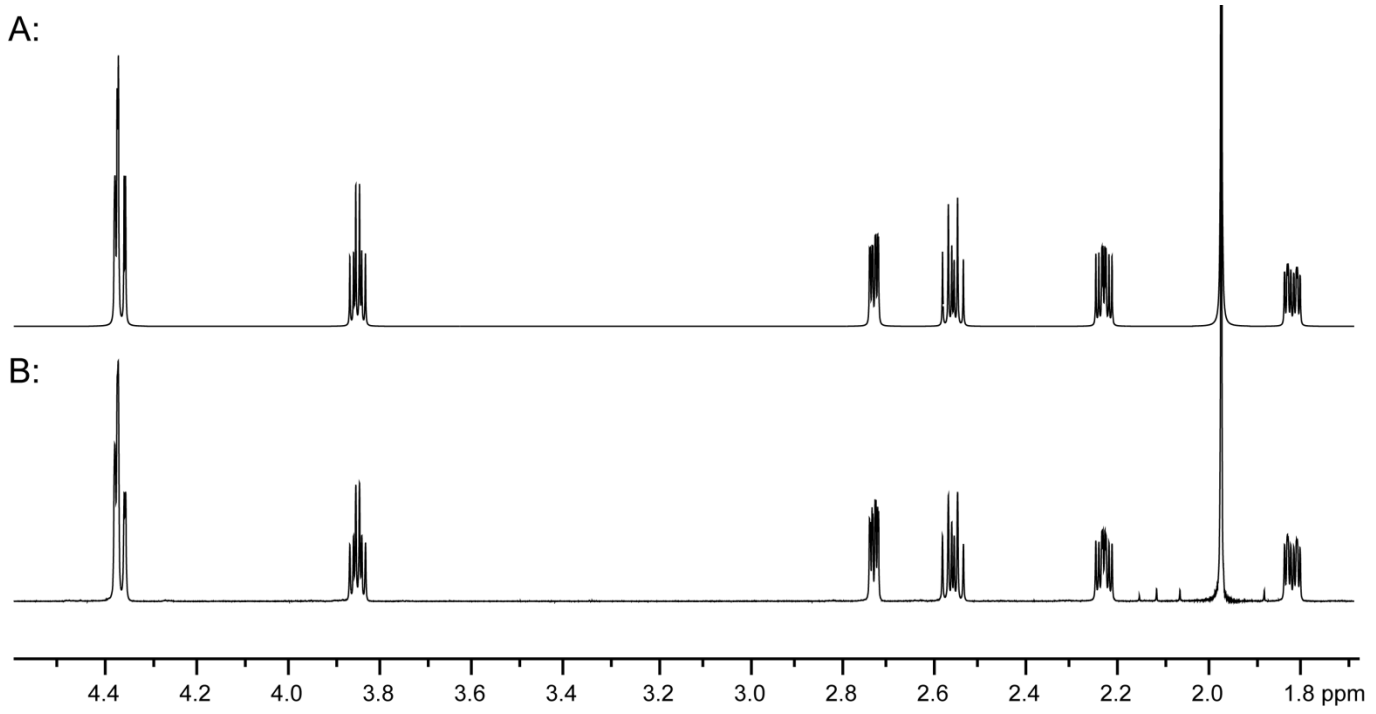

Figure S5. Comparison of simulated and measured ^{1}H NMR spectra for peramivir. **A:** The ^{1}H NMR spectrum for peramivir simulated in SpinWorks.[S6] **B:** The experimental ^{1}H NMR spectrum for peramivir in D_2O at 700 MHz. The RMS difference between the two spectra is 0.003 Hz.

Figure S6: nOe Data for Peramivir (D_2O, 500 MHz)

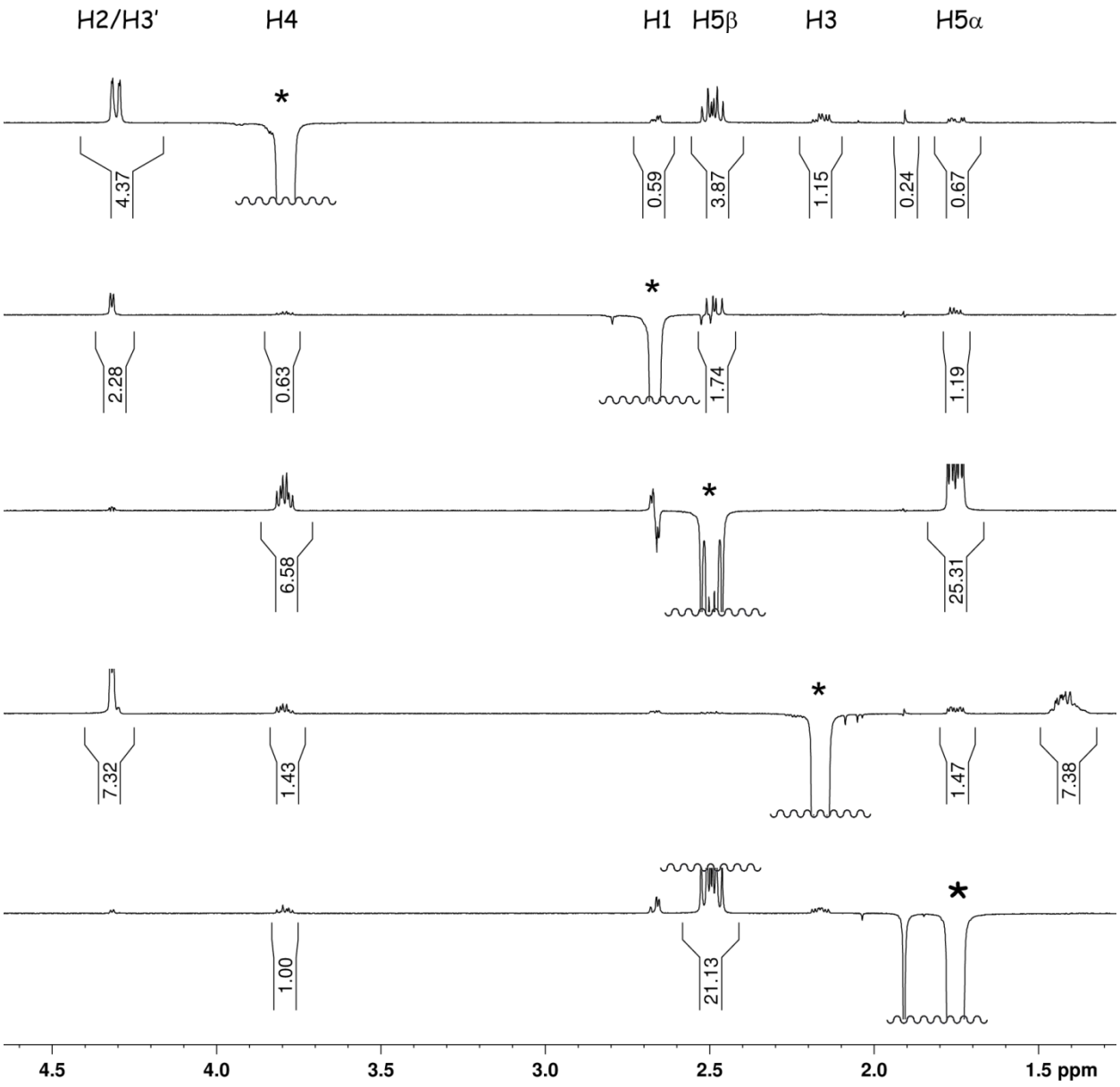

Figure S6. nOe data for peramivir in D_2O at 500 MHz, using a D1 relaxation delay of 2 s, and a D8 mixing time of 0.65 s. Asterisks indicate the signal being irradiated. In each case, the integration of the irradiated signal was set to –100%.

Figure S7: Total Energy of MD Simulation of Peramivir

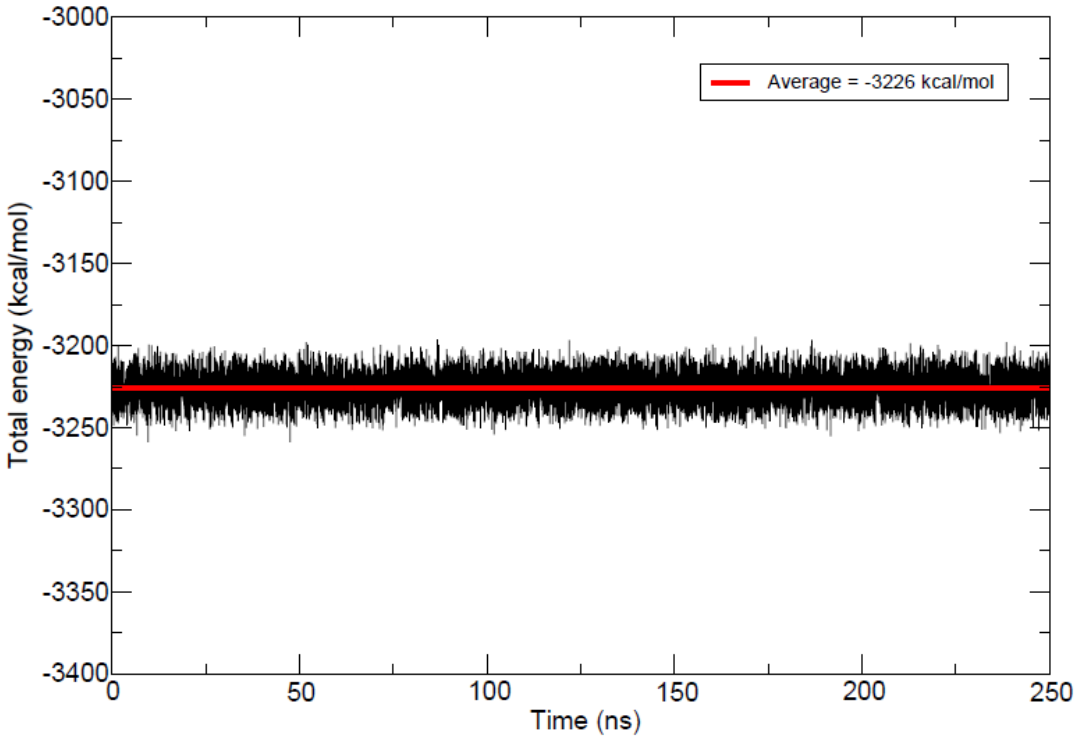

Figure S7. Total energy plotted over the course of the MD simulation of peramivir. The average energy (red line) is –3226 kcal/mol.

Figure S8: Histogram of Peramivir Ring Pucker

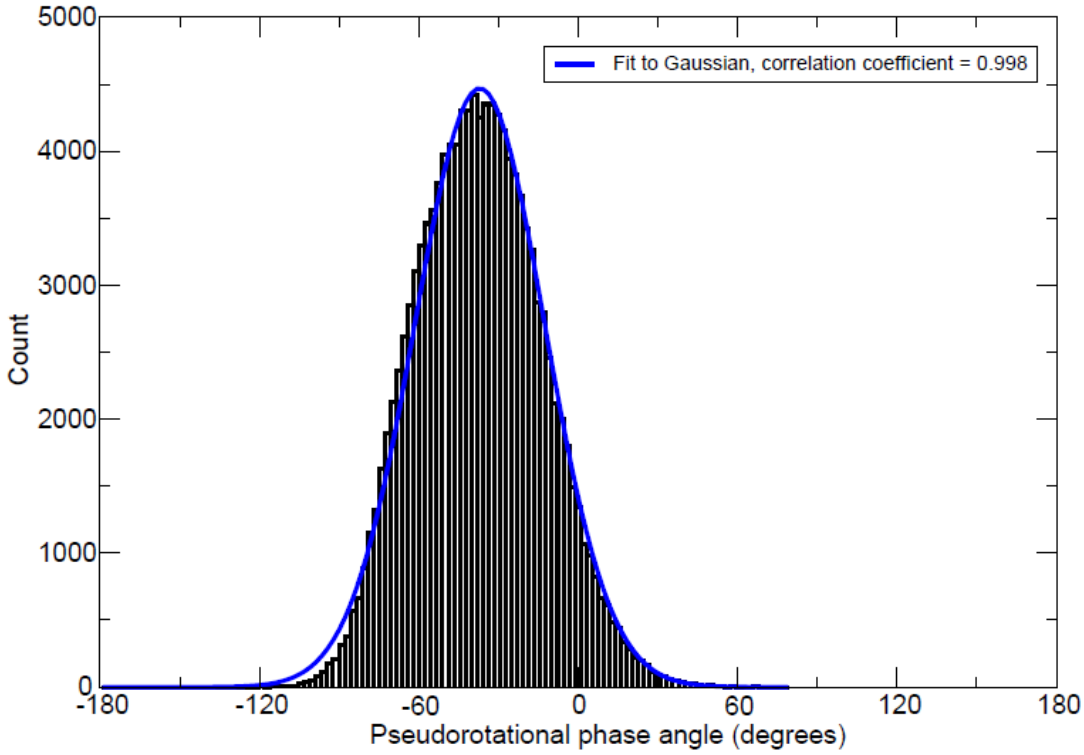

Figure S8. Histogram of pseudorotational phase angles, *P*, from the MD simulation of peramivir. The histogram can be fit to a Gaussian function (blue line), centered at $P = -37°$.

Table S1: Calculated and Experimental Scalar Couplings of Peramivir

	Experimental[a] (Hz)	Average from MD simulation (Hz)	Average from the X-ray[b] (Hz)	Bound in H1N9[c] (Hz)
$^3J_{H1,H2}$	1.3	0.7 ± 0.9	1.1 ± 0.2	2.1
$^3J_{H1,H5\alpha}$	3.9	3.7 ± 2.9	0.9 ± 0.2	11.5
$^3J_{H1,H5\beta}$	8.6	9.5 ± 1.9	7.6 ± 0.7	10.2
$^3J_{H2,H3}$	4.6	5.4 ± 1.5	3.6 ± 0.4	5.9
$^4J_{H2,\ H5\alpha}$	0.7	0.5 ± 0.4	–0.3 ± 0.3	–0.6
$^3J_{H3,H3'}$	10.9	10.8 ± 1.7	8.4 ± 0.5	9.9
$^3J_{H3,H4}$	9.1	8.9 ± 2.1	5.1 ± 0.5	8.2
$^3J_{H3',pentyl}$	2.2	2.3 ± 1.4	2.4 ± 0.5	2.7
$^3J_{H4,H5\alpha}$	5.7	5.6 ± 3.1	1.4 ± 0.3	10.0
$^3J_{H4,H5\beta}$	9.0	11.0 ± 2.1	9.9 ± 0.2	7.3
$^2J_{H5\alpha,H5\beta}$	–14.1	–14.3 ± 4.4	–14.3 ± 0.2	–14.7

[a]From the Spinworks[S6] simulation (see Figure S5). The error in the experimental values is estimated to be ± 0.2 Hz.

[b]Average across the four conformations visible in the unit cell.[S1]

[c]Bound structure from PDB 1L7F.[S3]

Table S2: Cartesian Coordinates of Average Peramivir Structure from MD Simulations (PDB format)

```
REMARK                    PDB file generated by ptraj
ATOM      1  C1  PER     1      -0.398  14.673  17.211  0.00  0.00
ATOM      2  C3  PER     1      -1.532  13.955  18.002  0.00  0.00
ATOM      3  O2  PER     1      -1.228  13.293  18.953  0.00  0.00
ATOM      4  O3  PER     1      -2.655  14.191  17.778  0.00  0.00
ATOM      5  H3  PER     1      -0.884  15.390  16.546  0.00  0.00
ATOM      6  C4  PER     1       0.603  15.359  18.131  0.00  0.00
ATOM      7  H4  PER     1       0.717  16.388  17.784  0.00  0.00
ATOM      8  H5  PER     1       0.294  15.385  19.178  0.00  0.00
ATOM      9  C5  PER     1       1.944  14.627  18.036  0.00  0.00
ATOM     10  N1  PER     1       2.456  14.387  19.419  0.00  0.00
ATOM     11  C6  PER     1       3.436  15.099  20.021  0.00  0.00
ATOM     12  N2  PER     1       4.077  16.077  19.408  0.00  0.00
ATOM     13  H6  PER     1       4.633  16.761  19.909  0.00  0.00
ATOM     14  H7  PER     1       3.691  16.473  18.558  0.00  0.00
ATOM     15  N3  PER     1       3.747  14.801  21.231  0.00  0.00
ATOM     16  H8  PER     1       4.398  15.351  21.781  0.00  0.00
ATOM     17  H9  PER     1       3.374  13.976  21.688  0.00  0.00
ATOM     18  H10 PER     1       2.101  13.626  19.988  0.00  0.00
ATOM     19  H11 PER     1       2.604  15.119  17.317  0.00  0.00
ATOM     20  C2  PER     1       0.380  13.579  16.431  0.00  0.00
ATOM     21  O1  PER     1       0.830  14.116  15.192  0.00  0.00
ATOM     22  H1  PER     1       0.100  14.112  14.548  0.00  0.00
ATOM     23  H2  PER     1      -0.102  12.634  16.165  0.00  0.00
ATOM     24  C7  PER     1       1.614  13.288  17.359  0.00  0.00
ATOM     25  H12 PER     1       1.260  12.530  18.060  0.00  0.00
ATOM     26  C8  PER     1       2.896  12.801  16.537  0.00  0.00
ATOM     27  H17 PER     1       3.137  13.661  15.908  0.00  0.00
ATOM     28  C11 PER     1       2.661  11.557  15.610  0.00  0.00
ATOM     29  C12 PER     1       2.491  10.299  16.463  0.00  0.00
ATOM     30  C13 PER     1       1.753   9.123  15.732  0.00  0.00
ATOM     31  H18 PER     1       0.738   9.434  15.475  0.00  0.00
ATOM     32  H19 PER     1       2.271   8.839  14.814  0.00  0.00
ATOM     33  H20 PER     1       1.941   8.295  16.419  0.00  0.00
ATOM     34  H21 PER     1       3.449   9.877  16.774  0.00  0.00
ATOM     35  H22 PER     1       1.917  10.484  17.373  0.00  0.00
ATOM     36  H23 PER     1       1.739  11.738  15.053  0.00  0.00
ATOM     37  C14 PER     1       3.841  11.432  14.558  0.00  0.00
ATOM     38  C15 PER     1       3.848  12.578  13.523  0.00  0.00
ATOM     39  H24 PER     1       4.676  12.569  12.811  0.00  0.00
ATOM     40  H25 PER     1       2.958  12.399  12.916  0.00  0.00
ATOM     41  H26 PER     1       3.845  13.538  14.043  0.00  0.00
ATOM     42  H27 PER     1       4.777  11.473  15.119  0.00  0.00
ATOM     43  H28 PER     1       3.698  10.423  14.165  0.00  0.00
ATOM     44  N4  PER     1       3.973  12.511  17.483  0.00  0.00
ATOM     45  H16 PER     1       3.874  11.789  18.181  0.00  0.00
ATOM     46  C9  PER     1       5.186  13.070  17.484  0.00  0.00
ATOM     47  C10 PER     1       6.099  12.510  18.518  0.00  0.00
ATOM     48  H13 PER     1       5.929  12.950  19.503  0.00  0.00
ATOM     49  H14 PER     1       5.987  11.424  18.495  0.00  0.00
ATOM     50  H15 PER     1       7.110  12.688  18.144  0.00  0.00
ATOM     51  O4  PER     1       5.506  13.915  16.686  0.00  0.00
```

Table S3: Energy and Cartesian Coordinates for DFT-Optimized Bound Peramivir

(Structure extracted from PDB 2HTU, and populated with hydrogens before minimization)

Optimization: DFT/B3LYP/6-31G* SCF total energy: –1108.3621629 hartrees

Coordinates:

	Atom		X	Y	Z
1	C	C5	2.0526027	1.6516706	0.0511530
2	C	C3	0.5336236	1.3647151	0.1235629
3	C	C15	0.4521766	-0.1478529	-0.2492441
4	C	C16	1.6940191	-0.7576748	0.4901903
5	C	C4	2.7302788	0.4000898	0.6368354
6	C	C6	4.1045634	0.1784927	0.0532626
7	O	O8	4.9676177	1.0261775	-0.0134829
8	C	C14	-0.8625688	-0.8967006	0.1564769
9	N	N5	-2.0423045	-0.2798106	-0.4316026
10	C	C13	-2.8821856	0.5333791	0.2821560
11	O	O14	-2.7483454	0.7776777	1.4744069
12	C	C7	-0.8354788	-2.4190016	-0.1927430
13	N	N1	-0.2387753	2.2084839	-0.7546335
14	C	C26	-0.7445892	3.4241837	-0.3123455
15	C	C11	-2.0009680	-3.1719233	0.4785723
16	C	C8	-0.7417682	-2.7139603	-1.7069979
17	H	H1	0.0895819	-2.7796909	0.2802599
18	H	H2	-1.7691322	-2.6702086	-2.1062928
19	H	H3	-0.2305683	-1.8889360	-2.2213436
20	C	C9	-0.0455027	-4.0236679	-2.0635129
21	H	H4	0.9419278	-4.0760409	-1.5990047
22	H	H5	0.0313479	-4.1399166	-3.1478599
23	H	H6	-0.6209306	-4.8881113	-1.7010188
24	H	H7	-2.9367430	-2.9699403	-0.0503561
25	H	H8	-1.7848336	-4.2466864	0.4175023
26	C	C12	-2.1723243	-2.8858156	1.9770234
27	H	H9	-2.6408928	-1.9118779	2.1754322
28	H	H10	-1.2273068	-2.8924856	2.5342278
29	H	H11	-2.8443521	-3.6252951	2.4363765
30	H	H12	-0.9063197	-0.7404456	1.2310800
31	C	C10	-3.9787822	1.2100443	-0.5290139
32	H	H13	-4.0074775	0.9291417	-1.5920469
33	H	H14	-3.8193790	2.2929962	-0.4907570
34	H	H15	-4.9617675	0.9958417	-0.0991930
35	H	H16	-2.1837335	-0.3355761	-1.4283106
36	H	H17	0.6369662	-0.2444566	-1.3265298
37	H	H18	2.0793005	-1.6283691	-0.0414194
38	O	O1	1.3828786	-1.1256098	1.8434630
39	H	H19	1.0271277	-2.0266101	1.8453391
40	H	H20	-0.0944269	2.2197385	-1.7551941
41	N	N2	-1.5105793	4.0596580	-1.3299782
42	H	H21	-2.0883228	3.4062194	-1.8488681
43	H	H22	-2.1263389	4.7810122	-0.9728898
44	H	H23	-0.8705069	4.8074755	1.0264611
45	N	N3	-0.4657809	3.8908931	0.8432101
46	H	H24	0.1552740	1.5282411	1.1331448
47	H	H25	2.8562477	0.4947733	1.7199288
48	H	H26	2.3312095	1.8054520	-0.9960883
49	H	H27	2.3183809	2.5478616	0.6190236
50	O	O2	4.3200982	-1.0887514	-0.4052049
51	H	H28	5.2511784	-1.0904986	-0.6962848

Table S4: Energy and Cartesian Coordinates for DFT-Optimized Unbound Peramivir (Structure extracted from CCDC 641049[1])

Optimization: DFT/B3LYP/6-31G* SCF total energy: –1108.3702293 hartrees

($\Delta\Delta H_f$ = –21.2 kJ/mol)

Coordinates:

	Atom		X	Y	Z
1	C	C10	0.1895236	-0.5782978	0.1182827
2	N	N7	-1.3504028	1.3064304	-0.3289997
3	C	C19	1.2626176	0.4654492	0.5486937
4	N	N1	1.7996406	1.1371759	-0.6329727
5	C	C11	2.3413901	-0.3342199	1.3526827
6	C	C13	2.0136037	-1.8214896	1.1632539
7	C	C20	0.4659582	-1.8043086	1.0153794
8	C	C9	-1.2649920	-0.0556078	0.1888325
9	C	C16	-2.3056263	-1.0114005	-0.4471920
10	C	C18	-3.7466475	-0.6158252	-0.0771128
11	C	C17	-2.1371389	-1.1249748	-1.9803169
12	C	C12	-1.6342827	2.3952310	0.4532684
13	C	C14	2.3789956	2.3806552	-0.5613851
14	C	C15	2.6264482	-2.5060035	-0.0453709
15	O	O26	-1.8824398	2.3088302	1.6512075
16	O	O28	2.4760569	-3.6815113	-0.3017982
17	H	H1	-2.1061397	-2.0086717	-0.0326682
18	H	H2	-2.2898269	-0.1479410	-2.4581484
19	H	H3	-1.1131566	-1.4496373	-2.2060168
20	H	H4	-4.0036654	0.3473779	-0.5414443
21	H	H5	-4.4310838	-1.3427255	-0.5353547
22	C	C7	-4.0536174	-0.5517620	1.4249497
23	H	H6	-5.1318766	-0.4336249	1.5910112
24	H	H7	-3.5598436	0.2955563	1.9104626
25	H	H8	-3.7356213	-1.4670430	1.9398704
26	C	C8	-3.0601205	-2.1531131	-2.6450130
27	H	H9	-4.0968536	-1.8221373	-2.7617940
28	H	H10	-3.0761298	-3.0958212	-2.0759446
29	H	H11	-2.6881575	-2.4355134	-3.6415076
30	H	H12	-1.4917894	0.0479427	1.2512610
31	H	H13	-1.1607757	1.4718349	-1.3067833
32	C	C6	-1.6108562	3.7405791	-0.2645982
33	H	H14	-1.5975840	3.6430632	-1.3558773
34	H	H15	-0.7259975	4.2906102	0.0648059
35	H	H16	-2.5058586	4.2958222	0.0211053
36	H	H17	0.4698965	-0.9225287	-0.8858020
37	H	H18	3.3346908	0.0027289	1.0449789
38	H	H19	2.2723820	-0.0728416	2.4133053
39	H	H20	2.3354136	-2.4099355	2.0282973
40	H	H21	0.8652008	1.2692289	1.1701910
41	H	H22	0.0975287	-2.7262466	0.5441330
42	O	O1	-0.1703713	-1.6147299	2.2710770
43	H	H23	-0.0670440	-2.4245416	2.7928856
44	H	H24	2.0451394	0.5339476	-1.4060807
45	H	H25	2.8127849	3.9486111	0.4281405
46	N	N2	2.5321263	2.9766006	0.5674050
47	N	N3	2.8189247	2.9059239	-1.8123910
48	H	H26	3.7841847	3.2175913	-1.7368582
49	H	H27	2.7972218	2.2093263	-2.5548412
50	O	O2	3.3214924	-1.6848182	-0.8840437
51	H	H28	3.6155000	-2.2689850	-1.6102839

References for the Supplementary Information:

(S1) Keller, E.; Kraemer, V. Crystal structure of the trihydrate of the neuraminidase inhibitor C15H28N4O4 (Peramivir), a potential influenza A/B and avian-influenza (H5N1) drug. *Z. Naturforsch., B: Chem. Sci*. **2007**, *62*, 983-987.

(S2) Russell, R. J.; Haire, L. F.; Stevens, D. J.; Collins, P. J.; Lin, Y. P.; Blackburn, G. M.; Hay, A. J.; Gamblin, S. J.; Skehel, J. J. The structure of H5N1 avian influenza neuraminidase suggests new opportunities for drug design. *Nature* **2006**, *443*, 45-49.

(S3) Smith, B. J.; McKimm-Breshkin, J. L.; McDonald, M.; Fernley, R. T.; Varghese, J. N.; Colman, P. M. Structural Studies of the Resistance of Influenza Virus Neuramindase to Inhibitors. *J. Med. Chem.* **2002**, *45*, 2207-2212.

(S4) Wu, Y.; Bi, Y.; Vavricka, C. J.; Sun, X.; Zhang, Y.; Gao, F.; Zhao, M.; Xiao, H.; Qin, C.; He, J.; Liu, W.; Yan, J.; Qi, J.; Gao, G. F. Characterization of two distinct neuraminidases from avian-origin human-infecting H7N9 influenza viruses. *Cell Res.* **2013**, 23, 1347-1355.

(S5) Oakley, A. J.; Barrett, S.; Peat, T. S.; Newman, J.; Streltsov, V. A.; Waddington, L.; Saito, T.; Tashiro, M.; McKimm-Breschkin, J. L. Structural and Functional Basis of Resistance to Neuraminidase Inhibitors of Influenza B Viruses. *J. Med. Chem.* **2010**, *53*, 6421-6431.

(S6) Marat, K. SpinWorks 3.1.8.1. *University of Manitoba, Manitoba, Canada* **2011**.

(S7) Richards, M. R.; Bai, Y.; Lowary, T. L. Comparison between DFT- and NMR-based conformational analysis of methyl galactofuranosides. *Carbohydr. Res.* **2013**, *374*, 103-114.

(S8) Wang, J. M.; Wolf, R. M.; Caldwell, J. W.; Kollman, P. A.; Case, D. A. Development and testing of a general amber force field. *J. Comput. Chem.* **2004**, *25*, 1157–1174.

(S9) Case, D. A.; Darden, T. A.; T.E. Cheatham, I.; Simmerling, C. L.; Wang, J.; Duke, R. E.; Luo, R.; Crowley, M.; Walker, R. C.; Zhang, W.; Merz, K. M.; Wang, B.; Hayik, S.; Roitberg, A.; Seabra, G.; Kolossváry, I.; Wong, K. F.; Paesani, F.; Vanicek, J.; Wu, X.; Brozell, S. R.; Steinbrecher, T.; Golke, H.; Yang, L.; Tan, C.; Mongan, J.; Hornak, V.; Cui, G.; Mathews, D. H.; Seetin, M. G.; Saugi, C.; Babin, V.; Kollman, P. A. *AMBER 10*, Univeristy of California, San Francisco: **2008**.

(S10) Jorgensen, W. L.; Chandrasekhar, J.; Madura, J. D.; Impey, R. W.; Klein, M. L. Comparison of simple potential functions for simulating liquid water. *J. Chem. Phys.* **1983**, *79*, 926–935.

(S11) Seo, M.; Castillo, N.; Ganzynkowicz, R.; Daniels, C. R.; Woods, R. J.; Lowary, T. L.; Roy, P. N. Approach for the Simulation and Modeling of Flexible Rings: Application to the α-D-Arabinofuranoside Ring, a Key Constituent of Polysaccharides from Mycobacterium tuberculosis. *J. Chem. Theory Comput.* **2008**, *4*, 184–191.

(S12) Taha, H. A.; Castillo, N.; Roy, P.-N.; Lowary, T. L. Conformational Studies of Methyl β-d-Arabinofuranoside Using the AMBER/GLYCAM Approach. *J. Chem. Theory Comput.* **2009**, *5*, 430–438.

(S13) Bayly, C. I.; Cieplak, P.; Cornell, W.; Kollman, P. A. A well-behaved electrostatic potential based method using charge restraints for deriving atomic charges: the RESP model. *J. Phys. Chem.* **1993**, *97*, 10269–10280.

(S14) Hornak, V.; Abel, R.; Okur, A.; Strockbine, B.; Roitberg, A.; Simmerling, C. Comparison of multiple Amber force fields and development of improved protein backbone parameters. *Proteins* **2006**, *65*, 712–25.

(S15) Berendsen, H. J. C.; Postma, J. P. M.; Gunsteren, W. F. v.; DiNola, A.; Haak, J. R. Molecular dynamics with coupling to an external bath. *J. Chem. Phys.* **1984**, *81*, 3684–3690.

(S16) Ryckaert, J.-P.; Ciccotti, G.; Berendsen, H. J. C. Numerical integration of the cartesian equations of motion of a system with constraints: molecular dynamics of n-alkanes. *J. Comput. Phys.* **1977**, *23*, 327–341.

(S17) Becke, A. D. Density-functional thermochemistry. III. The role of exact exchange. *J. Chem. Phys.* **1993**, *98*, 5648–5652.

(S18) Rassolov, V. A.; Ratner, M. A.; Pople, J. A.; Redfern, P. C.; Curtiss, L. A. 6-31G* basis set for third-row atoms. *J. Comput. Chem.* **2001**, *22*, 976–984.

(S19) Frisch, M. J.; Pople, J. A.; Binkley, J. S. Self Consistent Molecular-Oribital Methods 0.25. Supplementary Functions for Gaussian-Basis Sets. *J. Chem. Phys.* **1984,** *80*, 3265–3269.

(S20) Frisch, M. J.; Trucks, G. W.; Schlegel, H. B.; Scuseria, G. E.; Robb, M. A.; Cheeseman, J. R.; Montgomery, J. A., Jr.; Vreven, T.; Kudin, K. N.; Burant, J. C.; Millam, J. M.; Iyengar, S. S.; Tomasi, J.; Barone, V.; Mennucci, B.; Cossi, M.; Scalmani, G.; Rega, N.; Petersson, G. A.; Nakatsuji, H.; Hada, M.; Ehara, M.; Toyota, K.; Fukuda, R.; Hasegawa, J.; Ishida, M.; Nakajima, T.; Honda, Y.; Kitao, O.; Nakai, H.; Klene, M.; Li, X.; Knox, J. E.; Hratchian, H. P.; Cross, J. B.; Bakken, V.; Adamo, C.; Jaramillo, J.; Gomperts, R.; Stratmann, R. E.; Yazyev, O.; Austin, A. J.; Cammi, R.; Pomelli, C.; Ochterski, J. W.; Ayala, P. Y.; Morokuma, K.; Voth, G. A.; Salvador, P.; Dannenberg, J. J.; Zakrzewski, V. G.; Dapprich, S.; Daniels, A. D.; Strain, M. C.; Farkas, O.; Malick, D. K.; Rabuck, A. D.; Raghavachari, K.; Foresman, J. B.; Ortiz, J. V.; Cui, Q.; Baboul, A. G.; Clifford, S.; Cioslowski, J.; Stefanov, B. B.; Liu, G.; Liashenko, A.; Piskorz, P.; Komaromi, I.; Martin, R. L.; Fox, D. J.; Keith, T.; Al-Laham, M. A.; Peng, C. Y.; Nanayakkara, A.; Challacombe, M.; Gill, P. M. W.; Johnson, B.; Chen, W.; Wong, M. W.; Gonzalez, C.; Pople, J. A. *Gaussian 03* Revision C.02; Gaussian, Inc.: Wallingford, CT, **2004**.

(S21) Bally, T.; Rablen, P. R. Quantum-Chemical Simulation of 1H NMR Spectra. 2.† Comparison of DFT-Based Procedures for Computing Proton–Proton Coupling Constants in Organic Molecules. *J. Org. Chem.* **2011**, *76*, 4818-4830.

(S22) Vavricka, C. J.; Li, Q.; Wu, Y.; Qi, J.; Wang, M.; Liu, Y.; Gao, F.; Liu, J.; Feng, E.; He, J.; Wang, J.; Liu, H.; Jiang, H.; Gao, G. F. Structural and functional analysis of laninamivir and its octanoate prodrug reveals group specific mechanisms for influenza NA inhibition. *Plos Pathog.* **2011**, *7*, e1002249-e1002249.

(S23) Naumov, P.; Yasuda, N.; Rabeh, W. M.; Bernstein, J. The elusive crystal structure of the neuraminidase inhibitor Tamiflu (oseltamivir phosphate): molecular details of action. *Chem. Commun.* **2013**, *49*, 1948-1950.

(S24) Xu, X.; Zhu, X.; Dwek, R. A.; Stevens, J.; Wilson, I. A. Structural characterization of the 1918 influenza virus H1N1 neuraminidase. *J. Virol.* **2008**, *82*, 10493-10501.

(S25) Macdonald, S. J. F.; Cameron, R.; Demaine, D. A.; Fenton, R. J.; Foster, G.; Gower, D.; Hamblin, J. N.; Hamilton, S.; Hart, G. J.; Hill, A. P.; Inglis, G. G. A.; Jin, B.; Jones, H. T.; McConnell, D. B.; McKimm-Breschkin, J.; Mills, G.; Nguyen, V.; Owens, I. J.; Parry, N.; Shanahan, S. E.; Smith, D.; Watson, K. G.; Wu, W.-Y.; Tucker, S. P. Dimeric Zanamivir Conjugates with Various Linking Groups Are Potent, Long-Lasting Inhibitors of Influenza Neuraminidase Including H5N1 Avian Influenza. *J. Med. Chem.* **2005**, *48*, 2964-2971.